

Automated Retinal Fovea Type Distinction in Spectral-domain Optical Coherence Tomography of Retinal Vein Occlusion

Jing Wu^a, Sebastian M. Waldstein^a, Bianca S. Gerendas^a, Georg Langs^b, Christian Simader^a and Ursula Schmidt-Erfurth^a

^aChristian Doppler Laboratory for Ophthalmic Image Analysis, Department of Ophthalmology and Optometry, Medical University of Vienna, Austria

^bComputational Imaging Research Lab, Department of Biomedical Imaging and Image-guided Therapy, Medical University of Vienna, Austria

ABSTRACT

Spectral-domain Optical Coherence Tomography (SD-OCT) is a non-invasive modality for acquiring high-resolution, three-dimensional (3D) cross-sectional volumetric images of the retina and the subretinal layers. SD-OCT also allows the detailed imaging of retinal pathology, aiding clinicians in the diagnosis of sight degrading diseases such as age-related macular degeneration (AMD), glaucoma and retinal vein occlusion (RVO).¹ Disease diagnosis, assessment, and treatment will require a patient to undergo multiple OCT scans, possibly using multiple scanners, to accurately and precisely gauge disease activity, progression and treatment success. However, cross-vendor imaging and patient movement may result in poor scan spatial correlation potentially leading to incorrect diagnosis or treatment analysis. The retinal fovea is the location of the highest visual acuity and is present in all patients, thus it is critical to vision and highly suitable for use as a primary landmark for cross-vendor/cross-patient registration for precise comparison of disease states. However, the location of the fovea in diseased eyes is extremely challenging to locate due to varying appearance and the presence of retinal layer destroying pathology. Thus categorising and detecting the fovea *type* is an important prior stage to automatically computing the fovea position.

Presented here is an automated cross-vendor method for fovea distinction in 3D SD-OCT scans of patients suffering from RVO, categorising scans into three distinct types. OCT scans are preprocessed by motion correction and noise filtering followed by segmentation using a kernel graph-cut approach. A statistically derived mask is applied to the resulting scan creating an ROI around the probable fovea location from which the uppermost retinal surface is delineated. For a normal appearance retina, minimisation to zero thickness is computed using the top two retinal surfaces. 3D local minima detection and layer thickness analysis are used to differentiate between the remaining two fovea types. Validation employs ground truth fovea types identified by clinical experts at the Vienna Reading Center (VRC). The results presented here are intended to show the feasibility of this method for the accurate and reproducible distinction of retinal fovea types from multiple vendor 3D SD-OCT scans of patients suffering from RVO, and for use in fovea position detection systems as a landmark for intra- and cross-vendor 3D OCT registration.

Keywords: automated fovea distinction, cross-vendor, 3D SD-OCT, retinal disease, multimodal registration

1. INTRODUCTION

Age-related macular degeneration (AMD), retinal vein occlusion (RVO), glaucoma and other sight threatening diseases can be imaged and identified using 3D SD-OCT of the eye, providing high resolution 3D cross-sectional images of the retinal structure. This allows the assessment of disease progression in the eye by allowing clinicians to track changes in retinal anatomical structures over time as well as between patients.

Further author information: (Send correspondence to Jing Wu)

Jing Wu: E-mail: jing.a.wu@meduniwien.ac.at, Telephone: +43(0)14040072460

An important image processing tool for this purpose is registration of retinal structures across different OCT scans and scanners. However, accurate and precise landmarks are required, of which the fovea is a highly suitable choice due to its consistent presence across all patients, consistency across time points, and being the functional centre of vision. However, the presence of pathology will affect the appearance of the retina and retinal layers, specifically around the location of the fovea. In order to accurately locate the fovea within pathological OCT scans, a distinction must be drawn between the fovea types as they each pose different challenges for detection. This work proposes and evaluates a novel method for retinal OCT fovea distinction on manually fovea centred 3D OCT scans featuring pathology.

The majority of work on fovea detection focusses primarily either on healthy or dry-AMD cases,² or detection of the fovea within the colour fundus image.³ RVO, both central (CRVO) and branch (BRVO), is a significant cause of blindness⁴ and the build-up of fluid filled cysts results in the deformation of the foveal region, thus fovea distinction and detection poses challenges unseen in the previously mentioned domains and as such, little work has been carried out in this area as far as we know.

The method for OCT scan pre-processing and fovea type distinction is described in the following section, followed by training and testing dataset description, and results dissemination and discussion.

2. METHODOLOGY

The presented method consists of two main steps, OCT scan preprocessing followed by fovea type distinction. We define an OCT volume as $\mathbf{V}(Z, X, Y)$ where Z is the axial, X the primary (B-scan, $\mathbf{B}_s(Z, X)$) and Y the secondary (A-scan, \mathbf{A}_s) scan directions as shown in Figure 1(a). For reference, the B-scan (Figure 1(b)) is otherwise known as the XZ plane, the plane perpendicular to the B-scan is the YZ (Figure 1(c)), and the en-face image (Figure 1(d)) is known as the XY plane as it is comprised of B-scan slices.

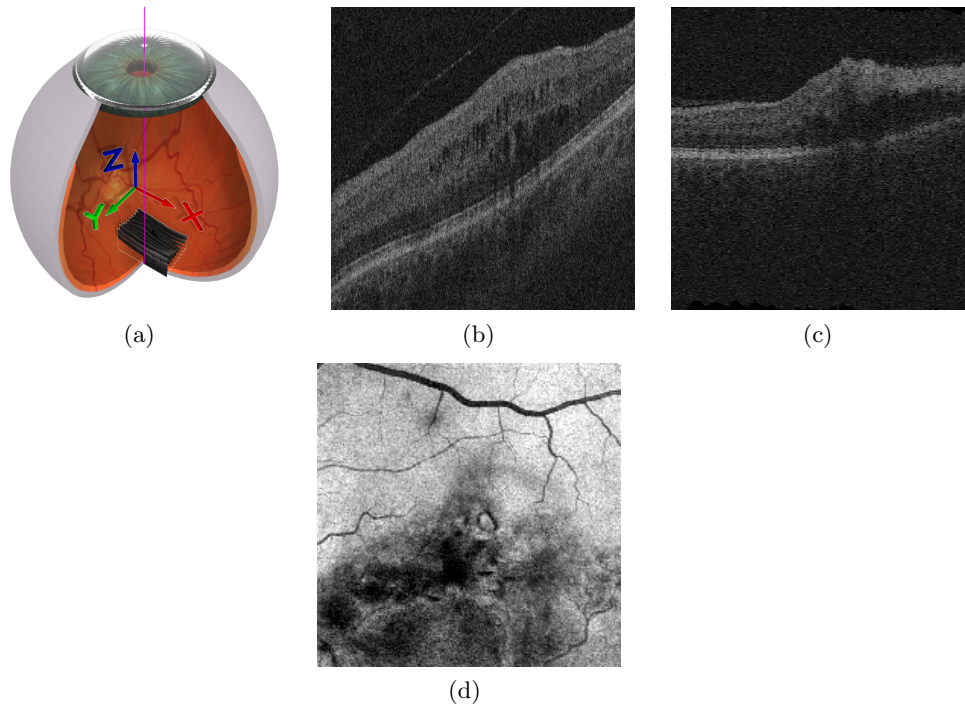


Figure 1. (a) Co-ordinate system of ophthalmic OCT scans.⁵ Exemplar retinal images of (b) B-scan (XZ) plane, (c) YZ plane, and (d) en-face (XY) plane.

2.1 Retinal SD-OCT Scan Preprocessing

Ophthalmic OCT scans are inherently affected by patient motion, thus the first preprocessing stage applied is motion correction in the Z plane. This aims to align the B-scans and compensate for the presence of

micro-saccades and patient movement as described by Montuoro et al.⁵ Firstly the position of the retina is determined by calculating the distance between the retinal pigment epithelium (RPE) and the top of the volume. The shift in the Z axis (δ_z) is then computed as required for removal of the movement artefacts in each B-scan. To compute δ_z , local curvature correction vectors are defined by estimating the local curvature using least-squares linear regression of two vectors extracted from a window around a given A-scan. Local curvature is then compensated for by shifting the A-scan according to the correction vector. Z motion correction is most visibly noticeable in the YZ plane as shown in Figure 2 where the pre and post motion corrected YZ planes are shown in Figures 2(a) and 2(b) respectively. The resulting Z motion corrected scan volume may appear tilted in the B-scan plane as seen in Figure 1(b). Fovea appearance is an important factor to consider for fovea distinction, thus tilt correction to in the X axis is beneficial. This is achieved by mapping the detected RPE to a sphere, shifting the corresponding retinal points. We denote the resulting Z motion corrected and tilt corrected volume as \mathbf{V}_C .

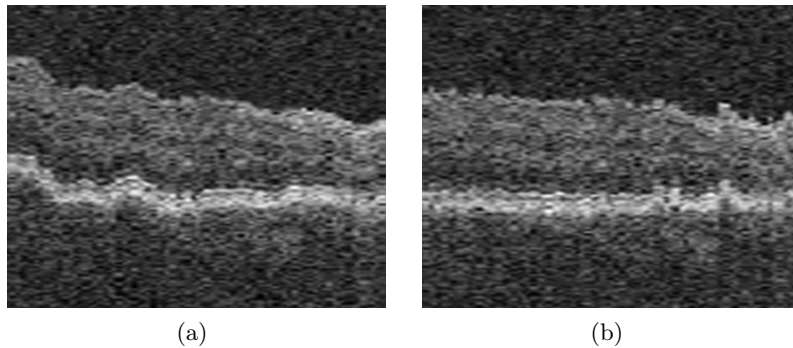


Figure 2. Exemplar Z motion correction showing (a) original YZ image, and (b) motion corrected image.

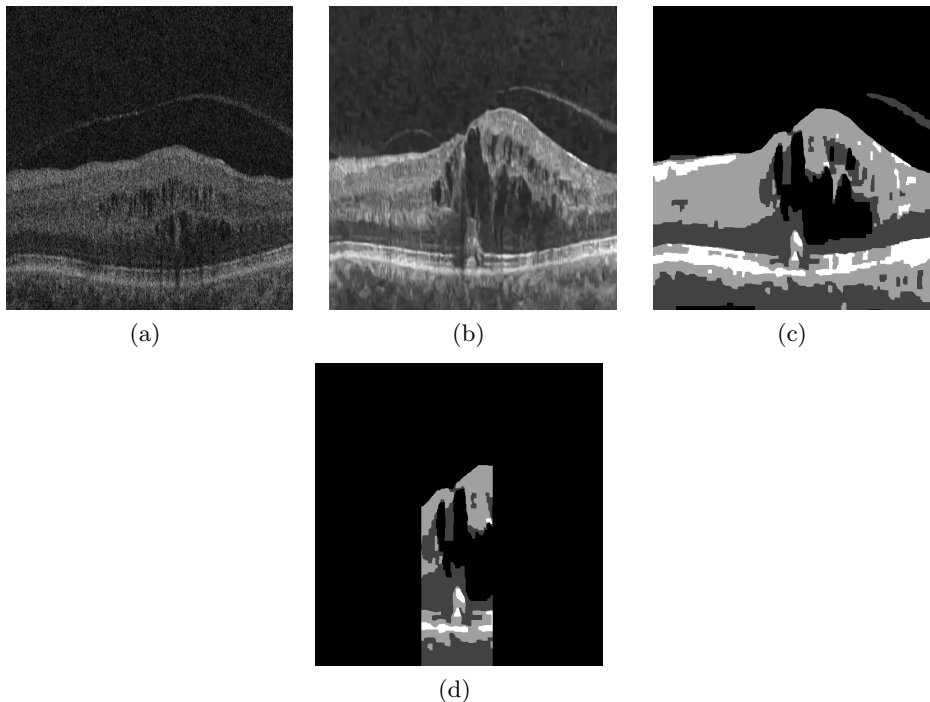


Figure 3. Exemplar intermediate processing stages (a) original B-scan, (b) noise filtered (a) using Dabov et al. method with $\sigma = 20$, (c) graph cut segmented (b), and (d) masked (c) using statistically derived generalised fovea location.

Within an OCT scan, there is a large degree of speckle noise which can affect the sharpness of the retinal

surfaces. We have shown the effectiveness of a sparse transform-domain collaborative filtering approach in a previous work⁶ originally presented by Dabov et al.⁷ and this method is used again here ($\sigma = 20$) resulting in the noise filtered, corrected OCT volume \mathbf{V}_{NF} , an example B-scan of which is shown in Figure 3(b).

Next, the top most surface, known as the inner limiting membrane (ILM) is delineated. The kernel graph cut based approach as described by Ben Salah et al.⁸ was applied to \mathbf{V}_{NF} using a smoothness constraint (0 .. 1) of 0.1, retaining any cavities in the fovea area. Distinct regions are segmented, regions of pathology to be distinguished from retinal layer tissue, tissue below the retina, and regions above the retina, giving \mathbf{V}_G (Figure 3(c)).

Given that the OCT scans in question are macular centred, the fovea is likely to be within a central region as seen in the XY plane. Thus by masking everything surrounding this region the likely fovea and corresponding distinctive features are localised (Figure 3(d)). \mathbf{V}_G is masked to a cylinder with height h along the Z axis, centred at (X, Y) , calculated based on the mean manually annotated fovea position from the complete data set of 484 OCT scans of RVO as a percentage of the OCT (X, Y) dimensions. The cylindrical radius r is calculated based on inspection of the fovea region from 50 randomly selected OCT scans from the previously mentioned dataset and is defined as $r_x = x_{sd} \times 4$, $r_y = (x_{sd}/R) \times 5$ where $R = X/Y$, sd is standard deviation when X and Y dimensions are disparate. When X and Y are equal, r_x only is used. We denote the masked \mathbf{V}_G as \mathbf{V}_{G_m} .

2.2 Fovea Type Distinction

We have categorised the fovea into three different types based on 60 RVO samples equally divided from the dataset mentioned previously. In the first case (Figure 4(a)) a normal depression is seen denoted as a normal foveal depression (NFD). There are then two diseased fovea appearance types⁹ where the fovea has been deformed by pathology such as cysts. Firstly a minor foveal depression (MFD, Figure 4(b)) and secondly an absent foveal depression (AFD, Figure 4(c)). This is further expanded for RVO as the AFD has a parabolic ILM appearance, thus we denote this as an absent foveal depression (AFD) as no depression is present.

In NFD cases, distinction is accomplished by examining the two uppermost surfaces of the retina, the ILM and the nerve fibre layer/ganglion cell layer (RNFL/GCL) respectively. At the fovea, these two surfaces meet and thus have a layer thickness of zero. We calculate this layer thickness for each B-scan in \mathbf{V} using the graph-cut retinal layer segmentation of Garvin et al.¹⁰ which can segment up to 11 retinal layers and has shown to perform well at delineating the ILM and RNFL in normal cases. If the ILM-RNFL/GCL layer thickness is found to be zero across at least 3 contiguous B-scans within \mathbf{V}_{G_m} , the scan is labelled as NFD. In all cases, NFD is the first examination to be performed.

Should the NFD distinction method fail to hold true, the following test is performed. From \mathbf{V}_{G_m} the ILM section within the masked region is delineated. A multi-step procedure is performed that firstly checks if the current B-scan $B_n \in \mathbf{V}_G$. If true, region growing is performed on B_n from a point just above the ILM surface delineated using the method of Garvin et al. Edge detection is performed on the resulting segmented region R_{B_n} from which geometric conditions are used to filter the edges not pertaining to the ILM. This gives the ILM_{B_n} , the ILM segment for B_n . This procedure is repeated for B-scans within \mathbf{V}_{G_m} resulting in a matrix of values representing the masked ILM surface points, $mILM_{B_n}$. Local minima detection is then employed to locate all candidate troughs on this surface ($mILM_{B_n}$) as exemplified in Figure 4(e) where a small depression is visible between two conical peaks. In the event of multiple local minima, we introduce a continuity check step similar to the contiguous B-scan examination mentioned for the NFD case to distinguish between candidates. This step filters out candidate local minima disconnected from one another as anatomically, we know that the small foveal depression will be visible across numerous contiguous B-scans. Thus only candidate local minima with a maximum separation of 1 B-scans in the Y direction are retained. Should a minimum grouping of 3 contiguous candidate local minima be identified and given that the search has occurred within \mathbf{V}_{G_m} , the scan is labelled as MFD. Despite both types featuring a depression that varies in depth and width, the major distinction (for the NFD case) focusses on the presence of a contiguous region with zero thickness between the ILM and RNFL/GCL.

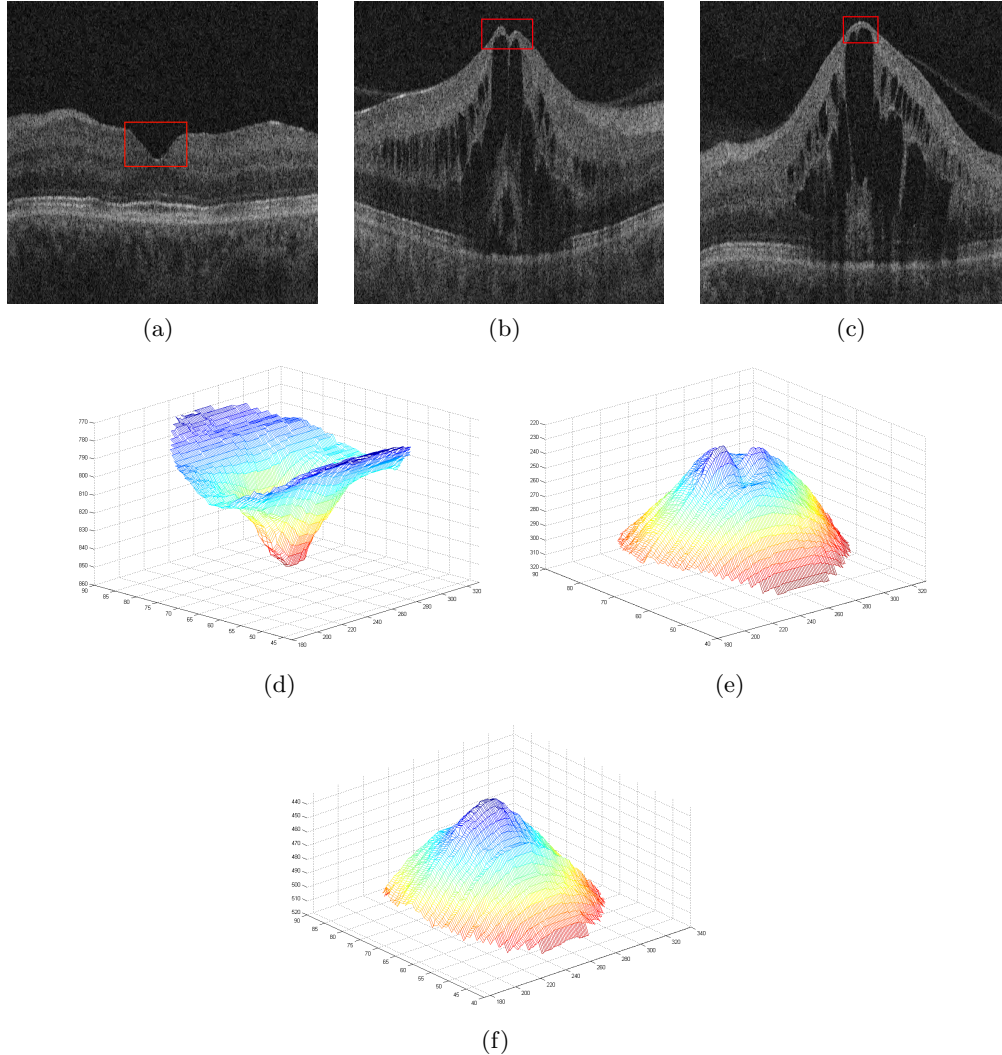


Figure 4. Exemplar fovea types (outlined in red) and masked ILM surface mesh for (a,d) NFD, (b,e) MFD and (c,f) AFD.

Finally for the AFD, firstly the two previous methods must not hold true. In order to distinguish the absence of a foveal depression, the ILM surface is assumed to be a parabola and as such features a global maximum within \mathbf{V}_{G_m} . Assessing the change in retinal thickness between the ILM and bottom surface known as the retinal pigment epithelium (RPE) from \mathbf{V}_{G_m} will show a smooth increase towards the central peak (seen in Figure 4(f)) which is unique to an AFD. Consequently, given a group of at least 3 contiguous B-scans each with a global maximum and surface conforming to this appearance within \mathbf{V}_{G_m} , the scan is labelled as an AFD volume.

3. DATASET

Retinal SD-OCT scans used in this work have been obtained from patients with central retinal vein occlusion (CRVO) and branch retinal vein occlusion (BRVO) acquired using three major scanner vendors Heidelberg Spectralis, Zeiss Cirrus, and Topcon 3D 2000. Scans include both eyes, disease related pathology and are manually fovea centred, thus not featuring the optic nerve head (ONH). Fovea centring was carried out by medical experts according to VRC guidelines for centre point re-plotting. As described previously, 484 OCT scans were used for construction of the likely fovea mask, from which 60 samples were chosen for

training of the fovea distinction step equally divided into the three fovea type categories. A further distinct set of 57 BRVO and 78 CRVO scans with ground truth fovea types are designated for testing. B-scan dimensions and composition varies by study and scanner protocol with the number of B-scans per volume ranging from 49 to 256. B-scan dimensions ranged from 496 to 1024 row pixels, and 200 to 512 column pixels. Thus slice thickness between contiguous B-scans also varies to a large degree as the same approximate physical volume is imaged.

4. RESULTS & VALIDATION

The data used for validation is comprised of 3D SD-OCT scans from 3 different vendor scanners (Heidelberg Spectralis, Zeiss Cirrus, and Topcon 3D OCT 2000), of which 57 are from patients with BRVO and 78 are from patients with CRVO.

Table 1. Comparison of ground truth fovea type distinctions with system results for BRVO.

| | | Ground truth | | | Total |
|--------|-----|--------------|----------|-----------|-------|
| | | NFD | MFD | AFD | |
| System | NFD | 19 | 1 | 1 | 21 |
| | MFD | 1 | 4 | 2 | 7 |
| | AFD | 0 | 0 | 29 | 29 |
| Total | | 20 | 5 | 32 | 57 |

Table 2. Comparison of ground truth fovea type distinctions with system results for CRVO.

| | | Ground truth | | | Total |
|--------|-----|--------------|-----------|-----------|-------|
| | | NFD | MFD | AFD | |
| System | NFD | 17 | 1 | 1 | 19 |
| | MFD | 0 | 14 | 3 | 17 |
| | AFD | 1 | 2 | 39 | 42 |
| Total | | 18 | 17 | 43 | 78 |

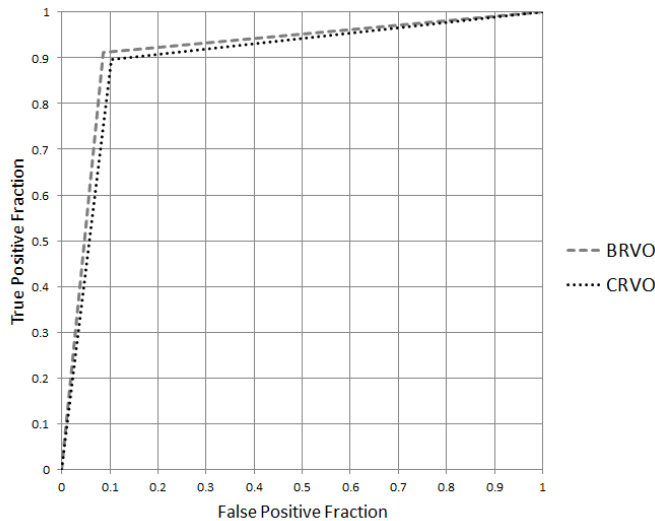


Figure 5. The resulting ROC curve of the fovea distinction results with area under the curve of 0.985.

Results of the fovea distinction algorithm for BRVO and CRVO are presented in Tables 1 and 2 respectively. From the 57 BRVO OCT scans tested, 52 fovea types (91%) were correctly distinguished in BRVO by

the system. A further 2 AFD fovea were identified as MFD, 1 AFD fovea as NFD, 1 MFD fovea as NFD, and finally 1 NFD as MFD. 70 fovea types (89%) were correctly distinguished by the system in the 78 CRVO OCT scans. A further 3 AFD fovea identified as MFD, 2 MFD fovea as AFD, 1 AFD fovea as NFD, 1 MFD fovea as NFD, and finally 1 NFD as AFD. The Receiver Operating Characteristic (ROC) curve in Figure 5 displays the aforementioned results with an area under the ROC curve (AUROC) of 0.9562 and 0.9487 for BRVO and CRVO respectively. Closer examination of the failure cases for BRVO show in the case where the system incorrectly classified a scan as NFD rather than AFD was the result of motion correction error resulting in layer segmentation error. The cases where the system classified a scan as either MFD or AFD rather than vice versa is the result of the strict smoothness constraint imposed by the retinal layer segmentation algorithm developed by Garvin et al.¹⁰ which, as demonstrated by these 2 cases, may not segment the ILM correctly in the presence of small depressions in a small minority of cases. Examination of the failure cases from the CRVO group corroborates the previous findings as 5 cases have been identified as MFD or AFD rather than vice versa. Again however, such issues occur in the small minority of cases.

5. CONCLUSIONS AND FURTHER WORK

An automated retinal fovea distinction method has been presented here for SD-OCT scans of patients suffering from RVO. Results show that for the scans tested, in the BRVO group, 91% of the fovea types were correctly distinguished. In the CRVO case, this figure was 89%. This represents a high level of system performance when applied to a test dataset comprised of multiple vendor scans that vary in appearance, image quality, and disease presence and quality. The small minority of failure cases were primarily related to the result of the pre-processing stage, specifically motion correction and/or layer segmentation. However, the few cases where this occurred were the result of heavily diseased scans where pathology caused inconsistencies of signal within the retina as well as extreme cases of anatomy deformation. In such cases, the presence of fluid filled cysts negatively affect the compositions and appearance of the retinal layers. Despite such cases being rare, an enhanced ILM segmentation algorithm that employs a more yielding smoothness constraint can improve segmentation accuracy of the ILM surface on which the depressions classifying MFD and AFD lay.

Further work aims to extend the fovea distinction algorithm to other diseases such as AMD and glaucoma where preliminary assessment has shown an extension of the ADF. In addition, the distinction algorithm will be further developed into an automated fovea point detection system in OCT. Given the difference in fovea position and appearance across the various fovea types, fovea type distinction allows fovea point detection algorithms to be developed for the specific fovea type. Consequently, fovea type distinction can be used to relate fovea appearance with disease state and pathology composition.

ACKNOWLEDGEMENT

The financial support of the Austrian Federal Ministry of Economy, Family and Youth and the National Foundation for Research, Technology and Development is gratefully acknowledged.

REFERENCES

1. W. Geitzenauer, C. K. Hitzenberger, and U. M. Schmidt-Erfurth, "Retinal optical coherence tomography: past, present and future perspectives," *Br J Ophthalmol* **95**, pp. 171–7, July 2010.
2. F. Wang, G. Gregori, P. J. Rosenfeld, B. J. Lujan, M. K. Durbin, and H. Bagherinia, "Automated Detection of the Foveal Center Improves SD-OCT Measurements of Central Retinal Thickness," *Ophthalmic Surgery, Lasers and Imaging Retina*, 2012.
3. M. V. Ibanez and A. Simó, "Bayesian detection of the fovea in eye fundus angiographies," *Pattern Recognition Letters*, 1999.
4. S. Rogers, R. L. McIntosh, N. Cheung, L. Lim, J. J. Wang, P. Mitchell, J. W. Kowalski, H. Nguyen, and T. Y. Wong, "The Prevalence of Retinal Vein Occlusion: Pooled Data from Population Studies from the United States, Europe, Asia, and Australia," *Ophthalmology*, 2010.

5. A. Montuoro, J. Wu, S. Waldstein, B. Gerendas, G. Langs, C. Simader, and U. Schmidt-Erfurth, "Motion Artefact Correction in Retinal Optical Coherence Tomography using Local Symmetry." in press, MICCAI.
6. J. Wu, B. S. Gerendas, S. M. Waldstein, C. Simader, and U. Schmidt-Erfurth, "Automated Vessel Shadow Segmentation of Fovea-centred Spectral-domain Images from Multiple OCT Devices," in *Proceedings of SPIE Medical Imaging*,
7. K. Dabov, A. Foi, V. Katkovnik, and K. Egiazarian, "Image denoising by sparse 3d transform-domain collaborative filtering," *IEEE Transactions on Image Processing* **16**, August 2007.
8. M. B. Salah, A. Mitiche, and I. B. Ayed, "Multiregion Image Segmentation by Parametric Kernel Graph Cuts," *IEEE Trans. on Image Proc.* , 2011.
9. C. A. Kiire, S. Broadgate, S. Halford, and N. V. Chong, "Diabetic macular edema with foveal eversion shows a distinct cytokine profile to other forms of diabetic macular edema in patients with type 2 diabetes," in *Proceedings of ARVO*,
10. M. K. Garvin, M. D. Abramoff, X. Wu, S. R. Russell, T. L. Burns, and M. Sonka, "Automated 3-D Intraretinal Layer Segmentation of Macular Spectral-Domain Optical Coherence Tomography Images," *IEEE Trans. on Medical Imaging* , 2009.